

Article

## Wheel Slip Control for Improving Traction-Ability and Energy Efficiency of a Personal Electric Vehicle

Kanghyun Nam <sup>1</sup>, Yoichi Hori <sup>2</sup> and Choonyoung Lee <sup>3,\*</sup>

<sup>1</sup> School of Mechanical Engineering, Yeungnam University, 280 Daehak-ro, Gyeongsan 712-749, Korea; E-Mail: khnam@yu.ac.kr

<sup>2</sup> Department of Advanced Energy, Graduate School of Frontier Sciences, the University of Tokyo, Kashiwa, Chiba 277-8561, Japan; E-Mail: hori@k.u-tokyo.ac.jp

<sup>3</sup> School of Mechanical Engineering, Kyungpook National University, 80 Daehak-ro, Bukgu, Daegu 702-701, Korea

\* Author to whom correspondence should be addressed; E-Mail: cylee@knu.ac.kr; Tel./Fax: +82-53-950-7541.

Academic Editor: Joeri Van Mierlo

Received: 20 May 2015 / Accepted: 30 June 2015 / Published: 7 July 2015

---

**Abstract:** In this paper, a robust wheel slip control system based on a sliding mode controller is proposed for improving traction-ability and reducing energy consumption during sudden acceleration for a personal electric vehicle. Sliding mode control techniques have been employed widely in the development of a robust wheel slip controller of conventional internal combustion engine vehicles due to their application effectiveness in nonlinear systems and robustness against model uncertainties and disturbances. A practical slip control system which takes advantage of the features of electric motors is proposed and an algorithm for vehicle velocity estimation is also introduced. The vehicle velocity estimator was designed based on rotational wheel dynamics, measurable motor torque, and wheel velocity as well as rule-based logic. The simulations and experiments were carried out using both CarSim software and an experimental electric vehicle equipped with in-wheel-motors. Through field tests, traction performance and effectiveness in terms of energy saving were all verified. Comparative experiments with variations of control variables proved the effectiveness and practicality of the proposed control design.

**Keywords:** electric vehicles; driving force observer; sliding mode control; vehicle velocity estimation

---

## 1. Introduction

Due to the increasing requirements with regard to introducing environmental-friendly vehicles and electrification of vehicle systems, much research on electric vehicles has been carried out [1–9]. In particular, in the motion control field of electric vehicles, traction control methods such as an anti-slip control [1], a model following control-based traction control [2], and slip ratio control based on slip estimation were proposed and applied in actual electric vehicles [3]. These traction control methods were developed based on the advantages of electric vehicles equipped with in-wheel motors. Moreover, in order to improve yaw stability of electric vehicles, various yaw moment control methods utilizing independent torque control were proposed by Fujimoto *et al.* [1]. The main advantages of electric vehicles in terms of motion control are summarized as follows [3–5]:

- Quick torque generation by in-wheel driving motors.
- Easy torque measurement from current sensing.
- Left and right independent wheel torque control.

In particular, since motor torques acting on each tire can be easily measured, we can accurately estimate the driving forces which are generated by tire-road interaction. These estimated driving forces can be widely used for estimating tire-road conditions, detecting wheel slip occurrence, and realizing the control law in motion control systems [5]. In this paper, a traction control method, by making the best use of the above advantages, is proposed and discussed. In general, the main objective of traction control is to prevent the degradation of driving performances, which occur during sudden acceleration under adverse road conditions. As a result, the traction-ability is greatly improved and the energy consumption by unnecessary wheel spin is also reduced in the case of electric vehicles.

The traction forces (also called as driving forces), generated by tire-road interaction, are expressed as a function of the wheel slip ratio, of the normal force acting in each wheel, and of the friction coefficient which depends on road conditions. Since the wheel slip ratio directly affects generation of the traction forces, the wheel slip ratio can be a control variable in the traction control system. Traction control methods based on wheel slip ratio control have been proposed and evaluated [6,10–12]. To realize these control methods, real-time information on rotational wheel velocity and vehicle velocity is required. Due to economic reasons, the vehicle velocity should be estimated using available sensors. In this paper, an algorithm for estimating the vehicle velocity is proposed, which is designed based on rule-based logic using measurable motor torques, rotational wheel velocity, and wheel dynamics.

In this paper, a sliding mode controller was adopted so as to make the control system robust against parameter uncertainties and disturbances. Additionally, the asymptotic stability property and robustness are discussed by employing the Lyapunov stability method. Sliding mode control techniques have been widely used in vehicle dynamics control systems such as anti-lock braking systems, yaw stability control systems, and traction control systems due to their strong robustness [10–24]. Since the vehicles operate under a wide range of speed and road conditions, the vehicle controllers should provide robustness

against varying parameters and undesired disturbances over all the driving regions. In [12], a second-order sliding mode traction controller for vehicles was presented to minimize tracking error. A sliding mode approach, based on conditional integrators, was proposed to control the wheel slip ratio in electric vehicles and its performances were verified through experimental results with a prototype electric vehicle [14]. In the literature [21], a sliding mode controller was designed to maintain the wheel slip at any given value and a sliding mode observer was used for obtaining the vehicle velocity for calculating the slip ratio. However, an additional sensor such as an acceleration meter was used and the gains of the sliding mode observer were chosen by trial and error.

The main contributions of this paper are given as follows:

- (1) design of a sliding mode wheel slip controller for improving traction performances of commercial electric vehicles equipped with in-wheel-motors;
- (2) development of the cost-free vehicle velocity estimator based on the measured motor torques and wheel velocities (which are obtained from the resolvers);
- (3) integration of the sliding mode controller and vehicle velocity estimator to actively control the driving wheels for avoiding wheel spin phenomenon;
- (4) implementation of the proposed traction control system on a commercial electric vehicle, shown in Figure 1.

This paper is organized as follows. An experimental electric vehicle equipped with in-wheel-motors is introduced in Section 2, which is followed in Section 3 by longitudinal vehicle dynamics modelling. In Section 4, the proposed traction control system including the sliding mode controller, a driving force observer, and the vehicle velocity estimator is presented. Computer simulations using the CarSim and experimental results are discussed in Section 5. The conclusion and future works are presented in Section 6.

## 2. Overview of an Experimental Electric Vehicle

A brief description of the experimental electric vehicle used in this work is recounted in this section. A commercial electric vehicle, named COMS, made by the Toyota Auto Body Company, Ltd., is a small-sized personal vehicle (see Figure 1) and has the following special features (see [5]):

- In-wheel motors (*i.e.*, interior permanent magnet synchronous motors) are mounted in the left and right rear wheels, respectively. Thus, each motor can be controlled independently.
- The control computer, which operates the traction control, is used for the realization of the developed control algorithms as well as the sensor signal processing.

The specifications and overall schematic of an experimental electric vehicle are listed in Table 1 and Figure 2, respectively.



Figure 1. Experimental personal electric vehicle.

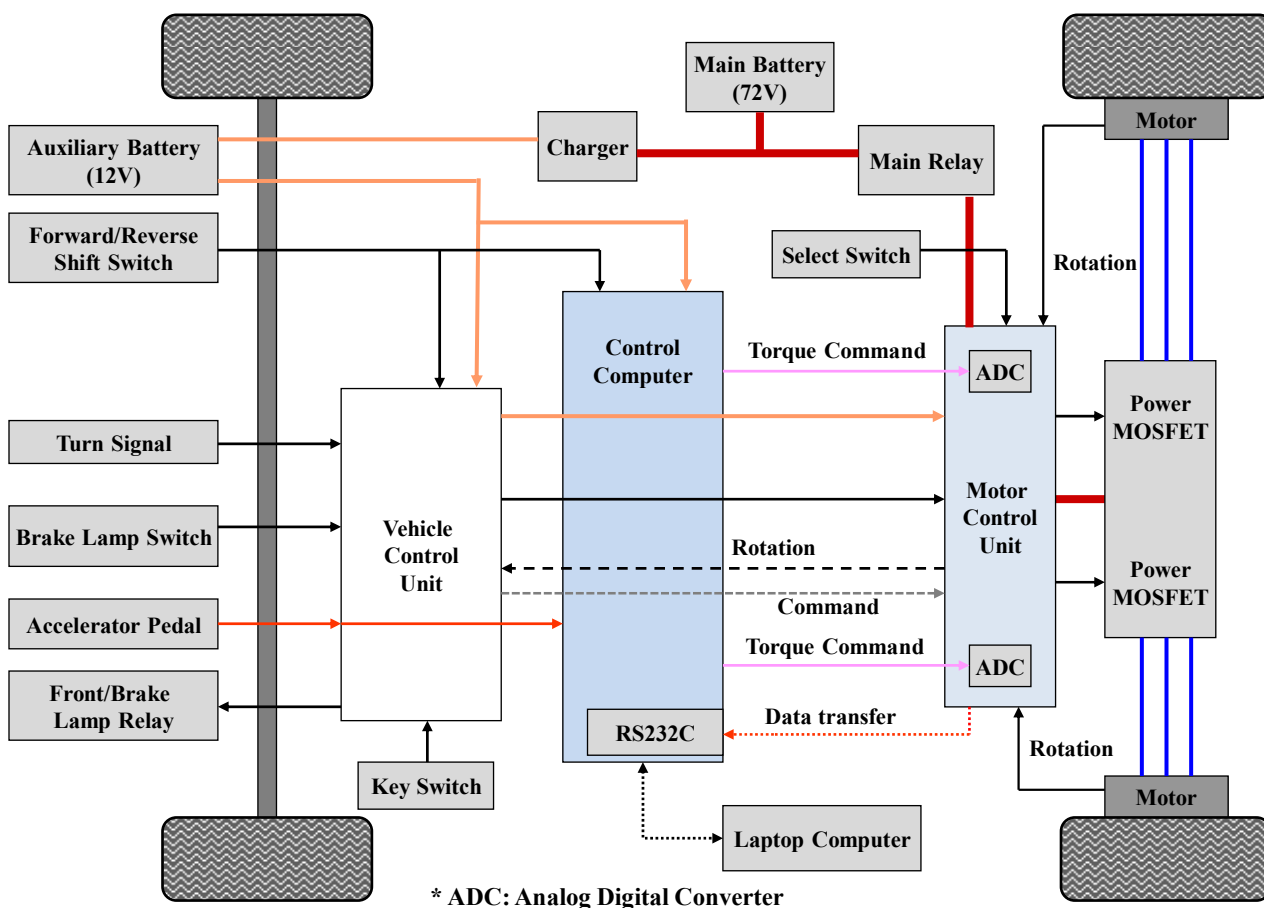


Figure 2. Schematic of the vehicle control system [5].

**Table 1.** Specifications of an experimental electric vehicle.

Driving Motor	2 Permanent Magnet Motors (Rear Wheels)
Maximum power	2 kW × 2
Maximum torque	100 Nm × 2
Total weight	360 kg
Wheel inertia	0.5 kg·m <sup>2</sup>
Wheel radius	0.22 m
Sampling time	0.01 s
Controller	PentiumM1.8G, ART-Linux
A/D and D/A	12 bit

### 3. Vehicle Model

A simple vehicle model, appropriate for longitudinal motion control, is described in Figure 3. A simple vehicle model representing the longitudinal dynamics can be obtained by assuming:

- Vehicle mass is distributed on each wheel equivalently.
- The lateral, yawing, pitch, and roll dynamics are neglected.

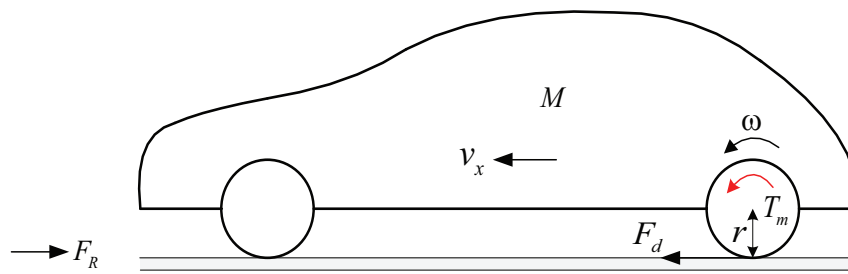


**Figure 3.** Longitudinal vehicle dynamics model.

The dynamic equations for the wheel rotating motion and longitudinal vehicle motion are as follows:

$$\text{Rotational wheel dynamics: } I_{\omega} \dot{\omega} = T_m - rF_d(\lambda, F_z) - T_b$$

$$\text{Longitudinal vehicle dynamics: } M\dot{v}_x = F_d - F_R \tag{1}$$

$$\text{Driving resistance: } F_R = F_{\text{air}}(v_x) + F_{\text{roll}} = c_x v_x^2 \text{sign}(v_x) + f_{\text{roll}} Mg$$

where  $\omega$  is the wheel angular velocity,  $v_x$  is the longitudinal velocity of the vehicle center of gravity,  $T_m$  is the driving input torque,  $T_b$  is the braking torque,  $F_d$  is the longitudinal tire-road contact force (also called as driving force),  $r$  is the wheel radius,  $I_{\omega}$  is the wheel moment of inertia,  $\lambda$  is the wheel slip ratio,  $M$  is the vehicle mass,  $F_{\text{air}}$  is the air drag resistance force,  $F_{\text{roll}}$  is the rolling resistance force,  $c_x$  is the longitudinal wind drag coefficient, and  $F_z$  is the normal force which can be calculated using available acceleration sensors.

When a driving motor torque  $T_m$  is applied to a pneumatic tire, the driving force will be developed at the contact patch between tire and road. At the same time, the tire tread of and within the contact patch is subject to compression during acceleration. The distance the tire travels when it is subject to a driving force will be less than when it is in free rotation. This phenomenon is referred to as the wheel

slip. The wheel slip is defined as the relative difference between a driving wheel’s angular velocity and the vehicle velocity [25], *i.e.*,

$$\lambda = \begin{cases} \frac{r\omega - v_x}{r\omega}, & r\omega > v_x \quad \text{for acceleration} \\ \frac{r\omega - v_x}{v_x}, & r\omega < v_x \quad \text{for deceleration} \end{cases} \quad (2)$$

The nonlinear wheel slip dynamics during acceleration is obtained by differentiating Equation (2) with respect to time and substituting it into Equation (1), thus obtaining:

$$\dot{\lambda} = \frac{-r\omega\dot{v}_x}{r^2\omega^2} + \frac{rv_x\dot{\omega}}{r^2\omega^2} \cong \frac{\dot{v}_x}{v_x}(\lambda - 1) + \frac{v_x}{I_\omega r\omega^2}(T_m - rF_d) + d \quad (3)$$

where  $d$  is defined as a lumped disturbance including terms related to driving resistances and parameter uncertainties. Also, since the only longitudinal motion during acceleration is considered in the control design, the braking torque  $T_b$  is neglected. The driving force  $F_d$  generated at each tire is the most important for deciding the longitudinal vehicle motion and is also a nonlinear function of the normal tire force  $F_z$ , of road friction coefficient  $\mu$ , and of wheel slip ratio  $\lambda$ . Figure 4 shows the typical relation curve between  $\lambda$  and  $F_d$  [25].

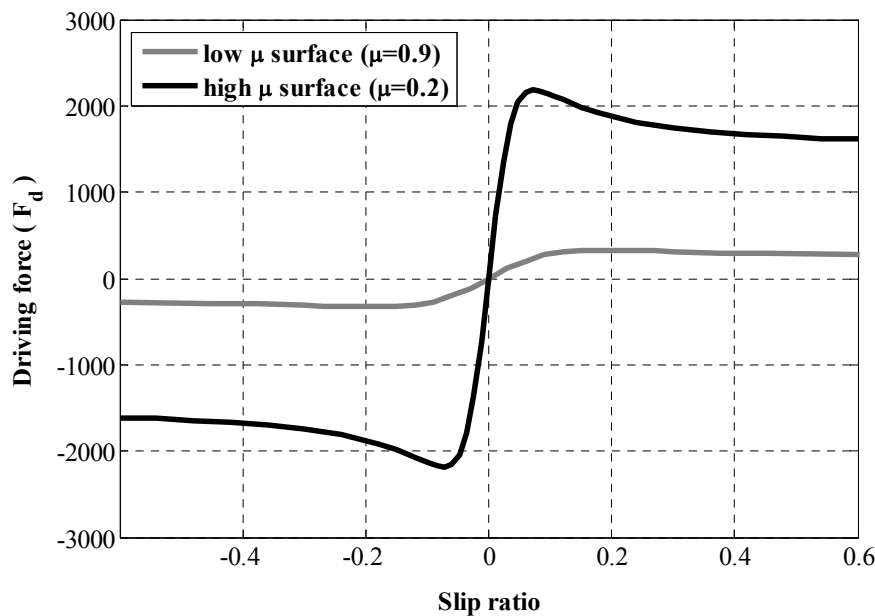


**Figure 4.** Relation curve between slip ratio ( $\lambda$ ) and driving force ( $F_d$ ).

#### 4. Design of a Traction Control System

##### 4.1. Overview of a Proposed Control System

In this section, a traction control system for an electric vehicle, equipped with in-wheel-motors, is introduced. The main objective of the traction control is to provide driving ability and stability without severe wheel slip. Figure 5 illustrates the block diagram of the proposed traction control system and the overall control scheme is given as:

- Feedback controller: a sliding mode control approach is applied to achieve robust tracking control of the wheel slip ratio and its asymptotical stability is proven by employing the Lyapunov function.
- Driving force observer: in order to monitor wheel status in real-time, a driving forces observer is designed based on rotational wheel dynamics and measurable motor torque and rotational wheel velocity.
- Vehicle velocity estimator: to realize the control law, generated from a sliding mode controller, real-time information on the vehicle velocity is required. A vehicle velocity estimator using rule-based logic is designed and evaluated by field test results.

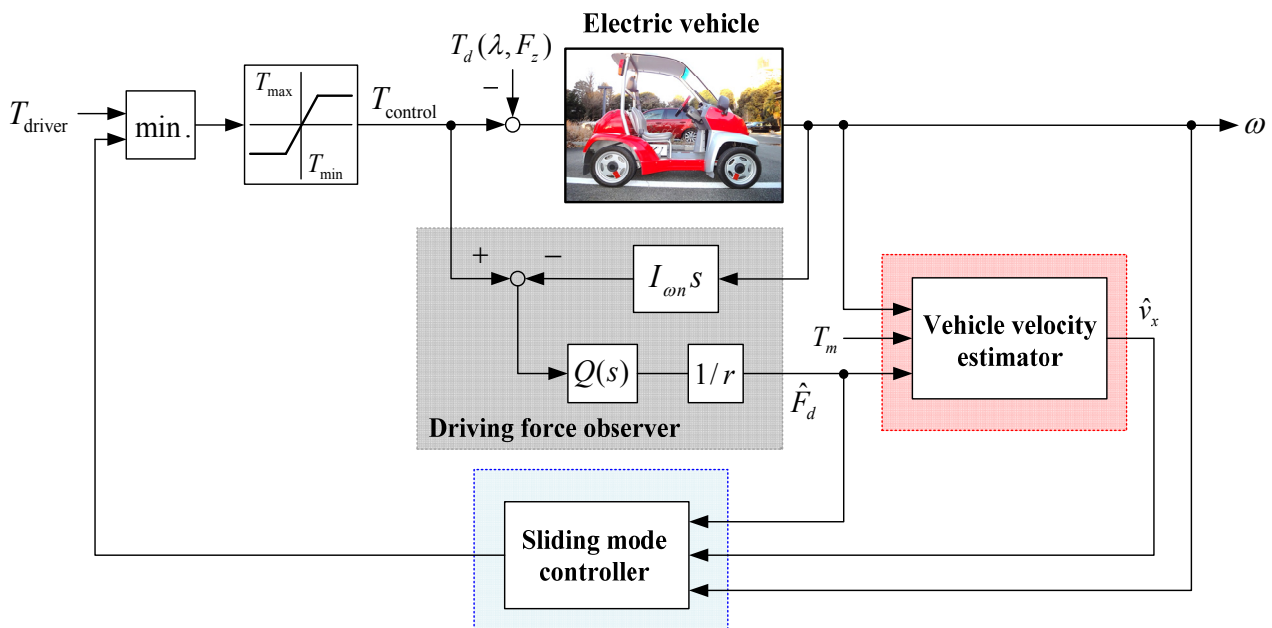


Figure 5. Overall structure of the proposed traction control system.

#### 4.2. Design of a Sliding Mode Controller

It is well known that sliding mode control is a robust control method to stabilize nonlinear and uncertain systems which have attractive features to keep the systems insensitive to the uncertainties on the sliding surface [26]. The conventional sliding mode control design approach consists of two steps. First, a sliding surface is designed such that the system trajectory along the surface acquires certain desired properties. Then, a discontinuous control is designed such that the system trajectories reach the sliding surface in a finite time. A sliding mode control as a general design technique for control systems has been well established, the advantages of a sliding model control method are: (1) fast response and good transient performance, (2) its robustness against a large class of perturbations or model uncertainties, and (3) the possibility of stabilizing some complex nonlinear systems which are difficult to stabilize by continuous state feedback laws [26,27]. Based on these advantages, sliding mode control approaches have been widely applied to vehicle dynamics control systems [14,15,27].

In this work, the main control objective is to track the desired wheel slip ratio which is pre-defined (*i.e.*,  $\lambda \rightarrow \lambda_d$ ). As aforementioned, the first step in sliding mode control design is to define the sliding surface. A sliding surface  $S(t)$  is defined as:

$$S(t) = \lambda - \lambda_d \tag{4}$$

Here we can see that the sliding condition  $S(t) = 0$  implies a zero tracking error. By designing a proper dynamics feedback control law, the trajectory of the closed loop system can be driven on the defined sliding surface (*i.e.*, Equation (4)) and evolve along it, and wheel slip ratio control can be achieved. In order to make the control performance achievable, a reaching condition is also designed as follows:

$$\dot{S} = -\beta S - K_S \cdot \text{sgn}(S) = -\beta(\lambda - \lambda_d) - K_S \cdot \text{sgn}(\lambda - \lambda_d) \tag{5}$$

where it is of note that by adding the proportional rate term  $-\beta S$ , the state is forced to approach the sliding surface faster when  $S$  is large enough [26]. The  $\beta > 0$  is a control parameter which determines the convergence rate of a tracking error, the  $K_S > 0$  is a control parameter which should be adjusted according to the number of uncertainties and disturbances [27].

By substituting wheel slip dynamics into the equation for a reaching condition (*i.e.*, Equation (5)), the sliding mode control law can be derived as follows:

$$T_{m,law} = r\hat{F}_d + \frac{I_\omega \omega \dot{v}_x}{v_x} + \frac{I_\omega r \omega^2}{v_x} \dot{\lambda}_d - \frac{I_\omega r \omega^2}{v_x} \beta(\lambda - \lambda_d) - \frac{I_\omega r \omega^2}{v_x} K_S \cdot \text{sgn}(\lambda - \lambda_d) \tag{6}$$

where it is difficult to accurately calculate the desired slip ratio  $\lambda_d$  in real-time because  $\lambda_d$  which is the optimal point generating the maximum driving force, is slightly different with respect to road conditions. In this work, the desired slip ratio is set to 0.01 for the high friction road and to 0.2 for the low friction road, respectively. Since we can easily detect the tire slip phenomenon from the driver’s torque command and the estimated driving force, a proposed wheel slip controller can work properly with a pre-defined desired slip ratio on a low friction road. It is of note that a discontinuous function  $\text{sgn}(\cdot)$  may lead to an undesirable chattering problem due to the measurement noise and some actuator delay. In order to attenuate this issue, the discontinuous control law term is replaced by a saturation function around the switching surface [27]. In addition, a simple low pass filter can be used for eliminating the high frequency chattering components.

We can prove that the sliding mode control law makes the closed-loop control system asymptotically stable by employing the Lyapunov function:

$$V = \frac{1}{2} S^2 \tag{7}$$

The time derivative of Equation (7) is:

$$\begin{aligned} \dot{V} = S\dot{S} &= S(\dot{\lambda} - \dot{\lambda}_d) = S \left[ \frac{\dot{v}_x}{v_x}(\lambda - 1) + \frac{v_x}{I_\omega r \omega^2} (T_{m,law} - rF_d) + d - \dot{\lambda}_d \right] \\ &= S[-\beta(\lambda - \lambda_d) - K_S \cdot \text{sgn}(\lambda - \lambda_d) + d] \\ &\leq -\beta S^2 - K_S |S| + |S| \cdot |d| \end{aligned} \tag{8}$$

where the lumped disturbance  $d$  is physically bounded and by defining  $\Phi = \sup_{t \geq 0} |d|$ , we find that if  $K_S$  is chosen as a larger value than that of  $\Phi$  (*i.e.*,  $K_S - \Phi > 0$ ),

$$\dot{V} \leq -\beta S^2 - K_s |S| + |S| \cdot |d| = -\beta S^2 - |S|(K_s - |d|) \leq -\beta S^2 - |S|(K_s - \Phi) < 0 \tag{9}$$

Thus, the control objective, *i.e.*,  $S(t) \rightarrow 0$  as  $t \rightarrow \infty$ , can be achieved by the derived control law (Equation (6)).

#### 4.3. Design of a Driving Force Observer

In a sliding mode control law (Equation (6)), a driving force  $\hat{F}_d$  is estimated from the driving force observer which is quite similar to the widely-used disturbance observer structure as shown in Figure 6b.

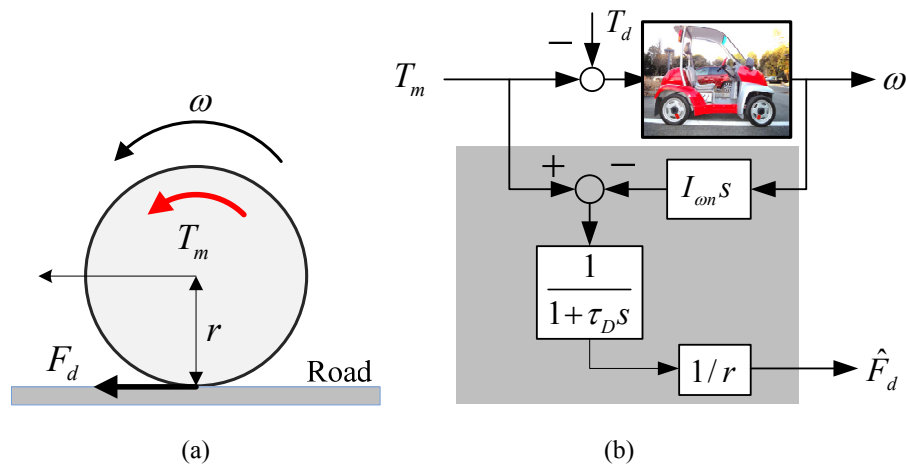


**Figure 6.** (a) Rotational wheel dynamics model. (b) Structure of a driving force observer.

By using the rotational wheel dynamics model (see Figure 6a) and a measurable motor torque as well as wheel velocity, it is easily estimated based on the following observer dynamics [28]:

$$\hat{F}_d = \frac{1}{1 + \tau_D s} \left( \frac{T_m - I_{on} \omega s}{r} \right) \tag{10}$$

where  $I_{on}$  is the nominal wheel inertia described in Table 1 and  $\tau_D$  is the time constant of the applied low-pass filter which rejects high frequency noises caused by a time derivative of  $\omega$ .

#### 4.4. Vehicle Velocity Estimation

In wheel slip control systems, it is necessarily required to detect vehicle velocity to calculate the wheel slip ratio. One of the common and most important issues in anti-slip control and traction control is the measurement of real-time estimation of the vehicle velocity over the ground. Since the vehicle velocity is always the basis for the wheel slip calculation, the vehicle velocity should be estimated using available sensor measurements so as to avoid cost increase. Many efforts have been focused on the practical issue of vehicle velocity estimation [29–32]. In [29], a fuzzy rule-based Kalman filtering technique, employing an additional accelerometer to complement the wheel-based velocity sensor, was proposed and its performance was verified through experiments using an actual vehicle. In [31], an adaptive nonlinear filtering approach was proposed to estimate the vehicle velocity by only using measurable wheel velocities. However, that adaptive algorithm was only tested off-line using real field-testing. In [32], nonlinear observers for both estimation of lateral and longitudinal velocity of

automotive vehicles were proposed and validated on experimental data from the test vehicle. Since a tire-road friction model has to be assumed, it is not practical for real application to the vehicles.

In this section, a vehicle velocity estimation algorithm based on the driving wheel’s velocity with an acceleration limiter is proposed. In addition, experiments were conducted using an actual electric vehicle to verify the proposed estimation strategy.

#### 4.4.1. Design of a Wheel Slip Indicator

The wheel slip indicator, which is defined as a ratio of the input torque and the estimated driving force, is expressed as:

$$\alpha = \frac{\text{Estimated driving force}}{\text{Motor command torque}} = \frac{\hat{F}_d}{T_m} \tag{11}$$

where  $T_m$  is a driver command torque (*i.e.*,  $T_m = T_{\text{driver}}$ , see Figure 5).

It is of note that we can see how severe the wheel slip condition was from the wheel slip indicator  $\alpha$ . As shown in Equation (11),  $T_m$  is the torque input to traction control system and  $\hat{F}_d$  is the result of tire-road interaction, which means system output. If we know both the input and output of the whole system, it is easy to predict the current status of the wheels. For example, when a vehicle runs on an asphalt road (non-slip condition), a wheel slip indicator  $\alpha$  converges to a certain value (see Equation (13)). Considering that the vehicle velocity is almost equal to the non-driving wheel’s velocity in the adhesive region, the longitudinal wheel dynamics (Equation (1)) can be idealized in the adhesive region and the transfer function from the motor torque input to the wheel rotational velocity is given by:

$$\frac{\omega(s)}{T_m(s)} = \frac{1}{(I_\omega + Mr^2)s} \tag{12}$$

The maximum wheel slip indicator  $\alpha_{\text{max}}$  is calculated in the adhesive region by a linear model (Equation (12)) for slip phenomenon:

$$\alpha_{\text{max}} = \frac{\hat{F}_d}{T_m} \approx \frac{M\dot{v}_x}{T_m} = \frac{Mrs\omega(s)}{T_m(s)} = \frac{Mrs}{(I_\omega + Mr^2)s} = \frac{Mr}{I_\omega + Mr^2}; \text{ in the adhesive region} \tag{13}$$

In the wheel slippery region, Equations (1) and (11) are used for calculating slip indicator:

$$\alpha = \frac{1}{r} \left( 1 - \frac{I_\omega \dot{\omega}}{T_m} \right) \Rightarrow \dot{\omega} = \left( \frac{1 - \alpha r}{I_\omega} \right) T_m; \text{ in the slippery region} \tag{14}$$

In order to identify the slip indicator  $\alpha$ , Equation (14) is rewritten in a parameter identification form as:

$$y[k] = \varphi^T[k]\theta[k] \tag{15}$$

where  $y[k] = \frac{\omega[k] - \omega[k-1]}{T_s}$ ,  $\varphi^T[k] = T_m[k]$ , and  $\theta[k] = \frac{1}{I_\omega}(1 - r\alpha[k])$ ,  $T_s$  is the sampling time.

A recursive least square (RLS) algorithm is used to estimate  $\alpha$  in real-time:

$$\begin{aligned} \hat{\theta}[k] &= \hat{\theta}[k-1] + L[k](y[k] - \varphi^T[k]\theta^T[k-1]) \\ L[k] &= \frac{P[k-1]\varphi[k]}{\varsigma[k] + \varphi^T[k]P[k-1]\varphi[k]} \\ P[k] &= \frac{1}{\varsigma[k]} \left( P[k-1] - \frac{P[k-1]\varphi[k]\varphi^T[k]P[k-1]}{\varsigma[k] + \varphi^T[k]P[k-1]\varphi[k]} \right) \end{aligned} \tag{16}$$

where  $L[k]$  is the Kalman gain,  $P[k]$  is the covariance matrix, and  $\varsigma[k]$  is a forgetting factor which is chosen to be a positive constant slightly smaller than 1. The smaller  $\varsigma[k]$  is, the less weight is assigned to the older data, which means that the past data are forgotten faster. In this work,  $\varsigma[k]$  around 0.995 was chosen to make reasonable tradeoff between noise sensitivity and tracking ability [33].

#### 4.4.2. Wheel Acceleration Limiter and Rule-Based Logic

The wheel acceleration limiter is designed for the purpose of obtaining the reference wheel velocity  $\tilde{v}_\omega$  which is the reasonable wheel velocity for calculating vehicle velocity within physical acceleration limit. Considering that limit values of the vehicle acceleration and deceleration depend on both motor power and vehicle weight, the acceleration limit value,  $A_{\text{acceleration}}$ , and deceleration limit value,  $A_{\text{deceleration}}$ , are chosen from the experimental data (*i.e.*,  $A_{\text{acceleration}} = 2.4 \text{ m/s}^2$ ,  $A_{\text{deceleration}} = -8 \text{ m/s}^2$  on high- $\mu$  road). These values are the maximum acceleration and deceleration which are obtained from field tests with an experimental electric vehicle. The mathematical expression for the rate limiter is given by:

$$A_{\text{deceleration}} \leq \frac{\tilde{v}_\omega[k+1] - \tilde{v}_\omega[k]}{T_s} \leq A_{\text{acceleration}} \tag{17}$$

The structure of a rate limiter is shown in Figure 7.

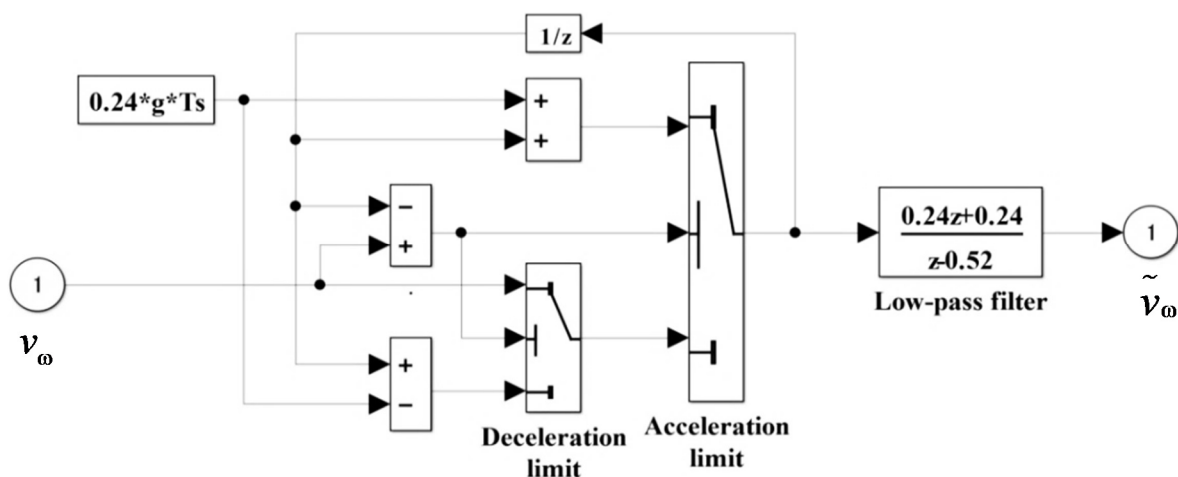


**Figure 7.** Structure of the rate limiter with a low pass filter.

In order to consider road friction and thereby variation in acceleration limit, the  $A_{\text{acceleration}}$  and  $A_{\text{deceleration}}$  are adapted based on a simple rule-based logic using a wheel slip indicator and control

activation level (CAL), which indicates the normalized control torque quantity (i.e., note that the severe slip control occurs in low-μ surface), defined as follows:

$$\text{Control activation level (CAL)} = \frac{T_{\text{driver}} - T_{\text{control}}}{T_{\text{driver}}} \tag{18}$$

$$\text{CAL} = \begin{cases} 1 & \text{if } T_{\text{control}} \approx 0 \quad (\text{severe slip control}) \\ 0 & \text{if } T_{\text{driver}} \approx T_{\text{control}} \quad (\text{no slip control}) \end{cases} \tag{18}$$

In this paper, the decision making rule is applied to detect vehicle state and to update the acceleration limit value. Figure 8 shows the decision making plot. Since the wheel slip control during acceleration is ultimately considered, the deceleration limit is chosen as a constant value:

$$\text{Decision rule: } \left( \begin{array}{l} \text{Rule: IF } \alpha_i < \alpha < \alpha_{i+1} \text{ and } \text{CAL}_i < \text{CAL} < \text{CAL}_{i+1} , \\ \text{THEN } A_{\text{acceleration}} = A(\cdot) \\ \text{where } 0.05\text{g} < A(\cdot) < 0.24\text{g} \text{ (i.e., } g = 9.81 \text{ m/s}^2) \end{array} \right) \tag{19}$$

where 0.05g is the maximum acceleration value on a significantly slippery road (i.e., μ = 0.2), 0.24g is the maximum acceleration value on a dry asphalt, both are obtained from field tests. The decision rule for updating the acceleration limit is very simple; based on calculated α and CAL, the status of wheel slip is easily recognized, according to the table shown in Figure 8, a physical limit value of the acceleration is updated in the rate limiter shown in Figure 7.

Finally, the vehicle velocity is calculated by averaging the left and right reference velocity (ṽ<sub>ω</sub>) of two rear wheels:

$$v_x = \frac{\tilde{v}_{\omega,\text{left}} + \tilde{v}_{\omega,\text{right}}}{2} \tag{20}$$

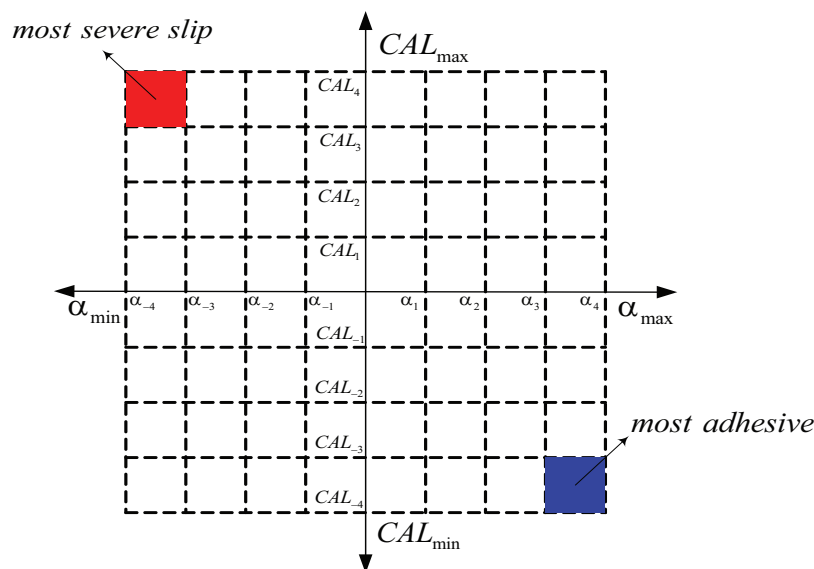


Figure 8. Rule-based decision making table for updating the acceleration limit.

#### 4.4.3. Experimental Results for Vehicle Velocity Estimation

In order to verify the performance of a proposed estimation algorithm, the experiments were carried out using an experimental electric vehicle (*i.e.*, COMS3). The driving conditions are given as follows (see Figure 9):

- Full acceleration without steering.
- Left wheel on high- $\mu$  surface and right wheel on high- $\mu$ /low- $\mu$ /high- $\mu$  transition surface.



**Figure 9.** Experiment conditions.

The experimental result for wheel acceleration limit adaptation is shown in Figure 10d. When a right wheel begins to slip (*i.e.*,  $t = 1.8$  s), an acceleration limit value for the right wheel, on low- $\mu$  surface, is reduced below 0.24g.

Figure 11 shows the results for vehicle velocity estimation. As shown in Figure 11b, the wheel velocity of the right wheel, controlled by a sliding mode controller, slightly oscillates to track the desired wheel slip ratio. In order to use the slipped wheel's velocity for estimating vehicle velocity, the slipped wheel's acceleration (*i.e.*, red-thin-line shown in Figure 11d) is processed as a magenta-dotted-line shown in Figure 11d by the rate limiter with a low pass filter as shown in Figure 7. Then, we can get the vehicle velocity by making use of the velocity of the processed left and right wheels as well as the decision making rules which are built based on field test data. From Figure 11a,b, we can confirm that the estimated vehicle velocity (*i.e.*, black line) is very close to the left wheel's velocity which is the non-slipped wheel's velocity.

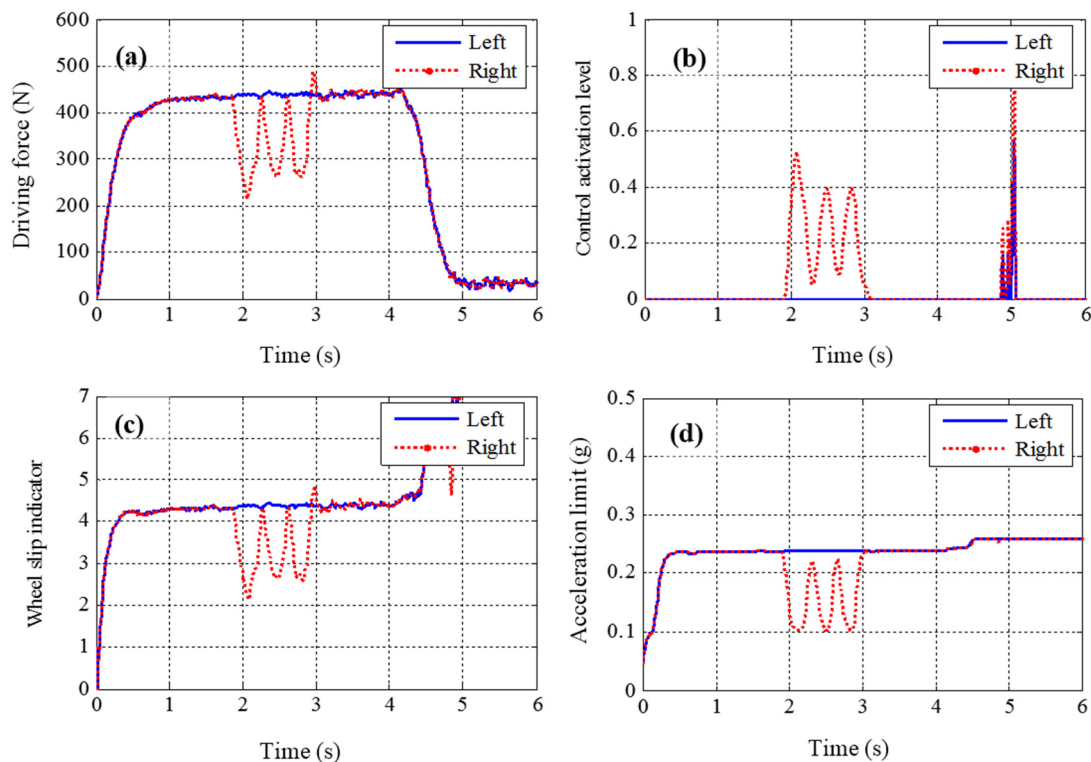


**Figure 10.** (a) Estimated driving force. (b) Control activation level obtained from Equation (18). (c) Wheel slip indicator (estimated from RLS algorithm). (d) Updated acceleration limit.

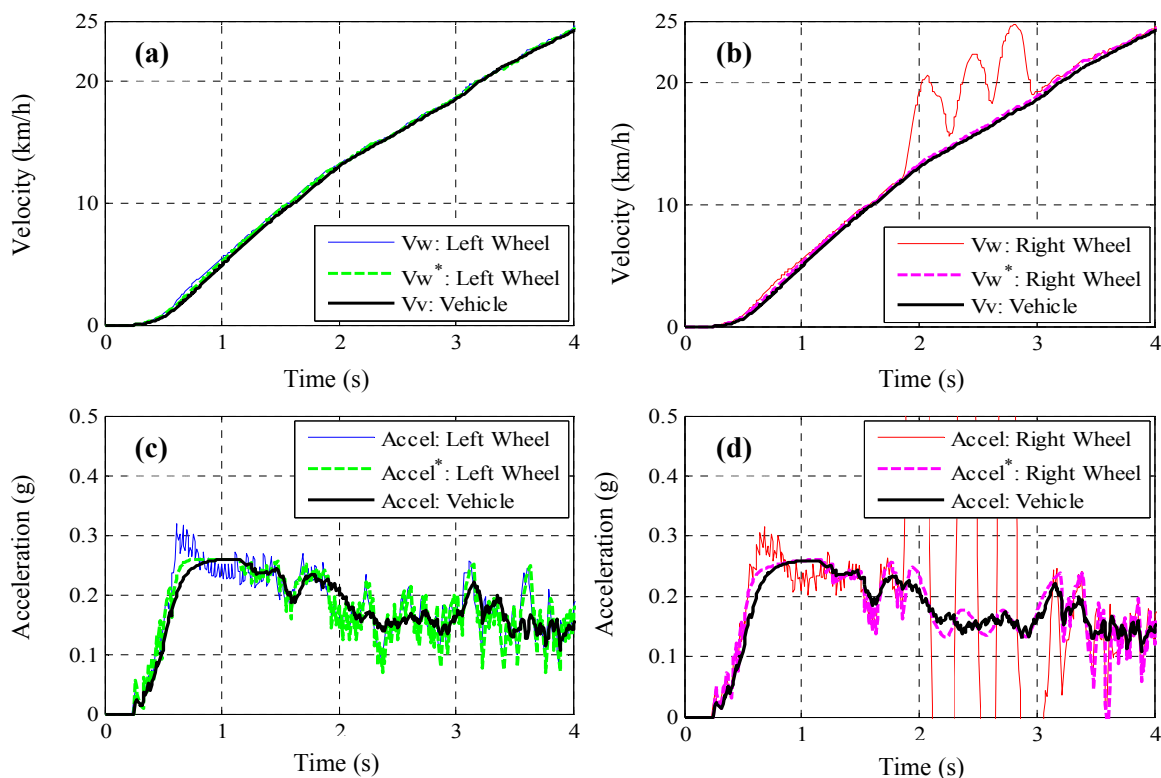


**Figure 11.** Experimental results for vehicle velocity estimation: (a) Left wheel velocity; (b) Right wheel velocity; (c) Left wheel acceleration; (d) Right wheel acceleration.

## 5. Computer Simulation and Experimental Verification

### 5.1. Computer Simulation Using a CarSim Software

Traction control and vehicle velocity estimation algorithms developed, in this work, were evaluated in a co-simulation using Matlab/Simulink and CarSim. The simulation model was built to match the values of the experimental electric vehicle and to consider nonlinear effects caused by time delay and disturbances. Full acceleration maneuvers, performed in a straight line and under slippery road conditions, were carried out to evaluate the control performance of the wheel slip controller (*i.e.*, sliding mode controller). Figure 12 shows the results of a sliding mode controller with different values of  $\beta$ . By analyzing the trajectory of wheel slip ratio shown in Figure 12b, it can be seen that the larger the  $\beta$ , the better the slip ratio tracking performance. Also, a direct relation can be observed between the settling time of the slip response and the  $\beta$  value.

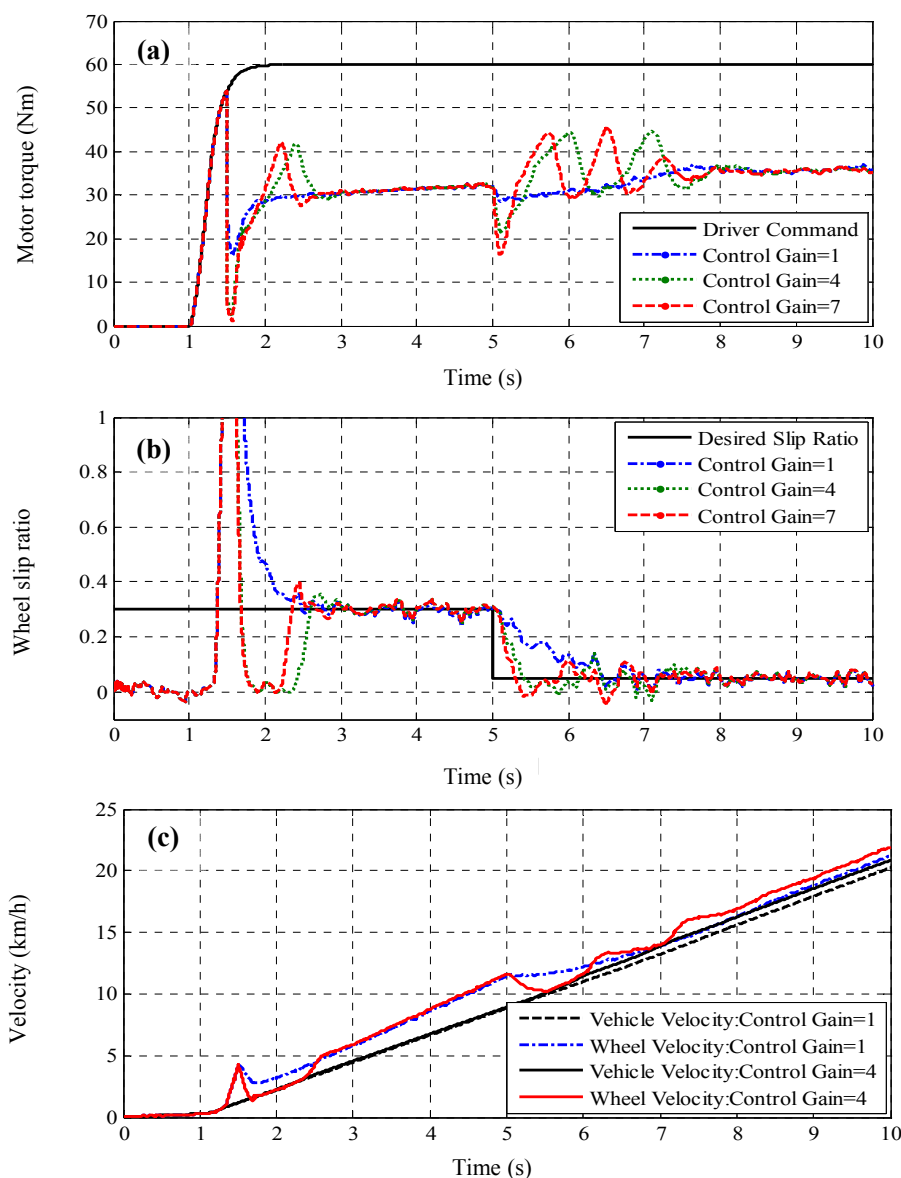


**Figure 12.** Simulation results for the proposed wheel slip controller (by CarSim software): (a) Motor torque; (b) Wheel slip ratio; (c) Wheel velocity and estimated vehicle velocity.

## 5.2. Experimental Verification

A proposed wheel slip controller implemented on an experimental electric vehicle equipped with in-wheel-motors is shown in Figure 1. Field tests were performed under the same driving conditions applied in the tests for evaluating the performance of the vehicle velocity estimation algorithm. In order to compare the results of both a with-control case and a without-control case, an experiment without a proposed controller was carried out and its result is shown in Figure 13.

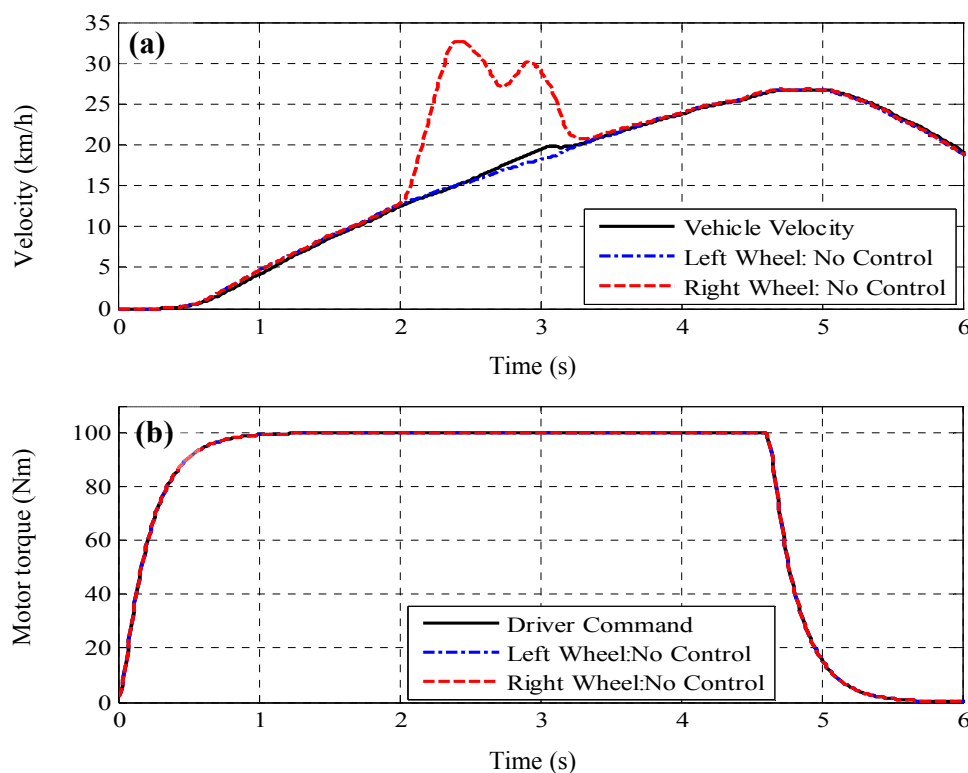


**Figure 13.** Experimental results without control: (a) Wheel velocity and estimated vehicle velocity; (b) Motor torque.

The slippery road was simulated by an acrylic sheet with water. An algorithm for vehicle velocity estimation was applied and the estimated vehicle velocity is shown in Figure 12 (*i.e.*, black line). When the vehicle enters a slippery road, a sudden wheel slip occurs, which can result in significant energy loss due to undesired wheel spin.

In the same manner, several experiments with a proposed wheel slip controller were carried out for evaluating the tracking performance of a proposed wheel slip controller and for confirming the effectiveness of traction control without using expensive vehicle velocity sensors.

The control parameter  $\beta$  which determines the convergence rate of the tracking error is set to 3 and 7, respectively. Moreover, the control parameter  $K_s$ , which should be adjusted according to the extent of uncertainties and disturbances, is set to a relatively small value to avoid undesired chattering in the wheel velocity.

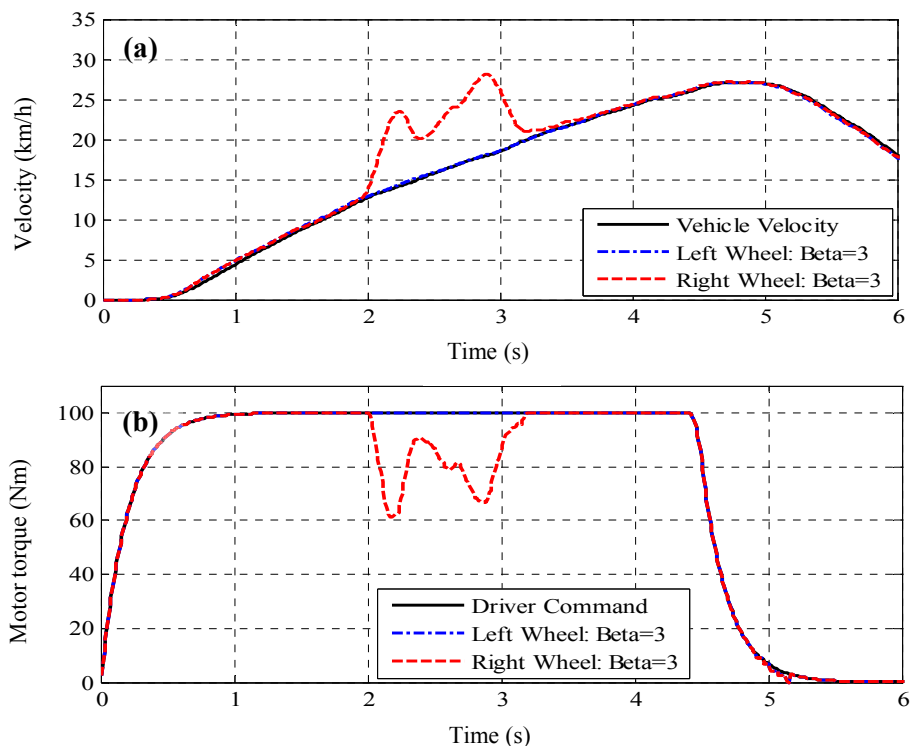


**Figure 14.** Experimental results with control (for  $\beta = 3$ ): (a) Wheel velocity and estimated vehicle velocity; (b) Motor torque.

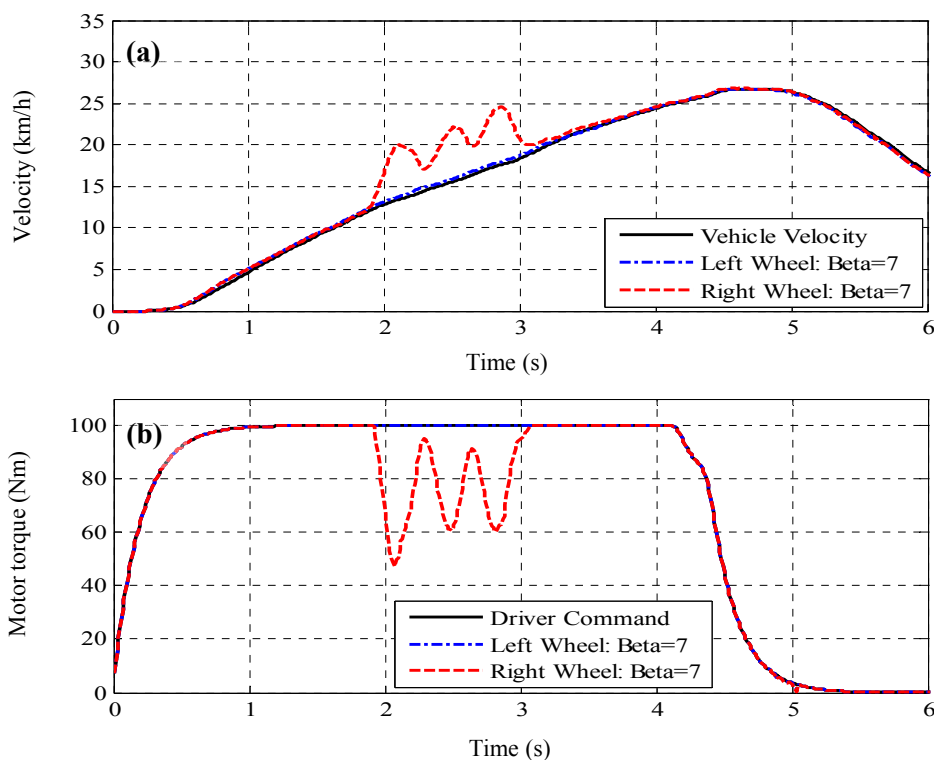


**Figure 15.** Experimental results with control (for  $\beta = 7$ ): (a) Wheel velocity and estimated vehicle velocity; (b) Motor torque.

Figures 14 and 15 show experimental results with different feedback gains. At  $t = 1.8$  s, a vehicle enters a slippery road, as shown in Figure 14a, due to the system delay, a sudden slip occurs in spite of

employing the slip controller, and then the proposed wheel slip controller begin to work normally. Figure 14b shows that, compared to the without-control case, the motor torque of the right wheel on a slippery road has decreased to avoid severe wheel slip. Here, it must be pointed out that, the quantity of decreased torque means less energy loss caused by undesired wheel slip on a slippery road. Therefore, both traction ability and reduction of energy consumption during acceleration on a slippery road are simultaneously achieved with the proposed wheel slip controller. Compared with the control results with  $\beta = 3$ , the result employing  $\beta = 7$  shows a better anti-slip performance as shown in Figure 16. The desired wheel slip ratio was set to 0.2 on a slippery road and the proposed sliding mode controller contributed to reduce the applied motor torque to minimize the tracking error.

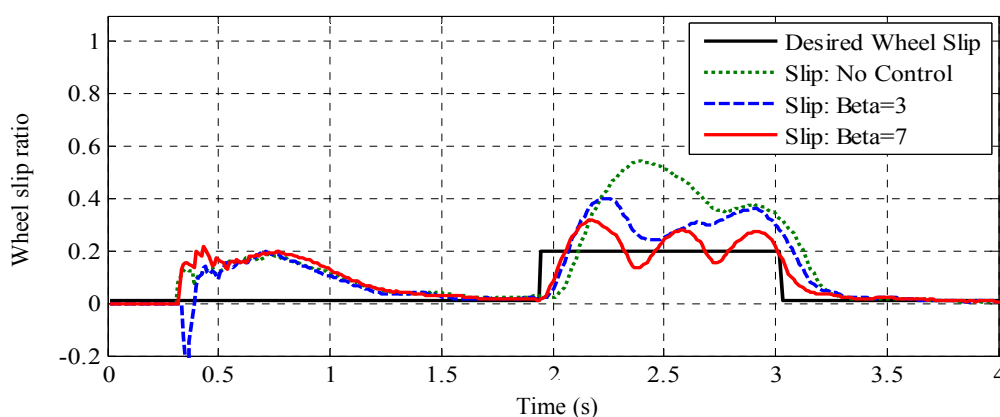


**Figure 16.** Experimental results for the proposed wheel slip controller: wheel slip ratio.

## 6. Conclusions

In this paper, a wheel slip controller, based on the sliding mode control approach, was proposed to improve the traction ability and to reduce energy loss while a vehicle accelerates on a slippery road. Moreover, an estimator of vehicle velocity was proposed and applied to the wheel slip control system. This vehicle velocity estimator, which makes use of only measurable motor torques and rotational wheel velocity, was realized based on a rule-based decision logic considering the driving limits of an experimental electric vehicle. Since the structure of the proposed algorithm is very simple and easily implementable, as well as being cost-free, it is expected that these algorithms will be applied to other control systems to enhance their control performance when vehicles run on a slippery road. The simulations and experiments indicate that a driving force observer-based sliding model controller, for the wheel slip control, works well to track the given desired wheel slip ratio. Although a slight oscillation in wheel velocity was observed, the anti-slip performance of the proposed controller was verified by analyzing the test results for both a with-control case and a without-control case. In addition, comparative simulations and experiments with variations of control parameters proved the effectiveness of the proposed estimator and control algorithms. In future work, we plan to apply the proposed algorithms to vehicle yaw stability control systems.

## Acknowledgments

This work was supported in part by the Yeungnam University Research Grant 215A580057, and in part by the National Research Foundation of Korea grant funded by Priority Research Centers Programs, NRF (2012-0005856), Basic Science Research Program, NRF (2011-0023437).

## Author Contributions

Kanghyun Nam and Hori Yoichi organized the overall control structure and contributed to the estimation algorithm design and experimental verification. Choonyoung Lee helped in the theoretical analysis of the proposed control system.

## Conflicts of Interest

The authors declare no conflict of interest.

## References

1. Fujimoto, H.; Fuji, K.; Takahashi, N. Traction and yaw-rate control of electric vehicle with slip-ratio and cornering stiffness estimation. In Proceedings of the American Control Conference, New York, NY, USA, 9–13 July 2007.
2. Hori, Y.; Toyoda, Y.; Tsuruoka, Y. Traction control of electric vehicle: Basic experimental results using the test EV “UOT electric march”. *IEEE Trans. Ind. Appl.* **1998**, *34*, 1131–1138.
3. Sakai, S.; Sado, H.; Hori, Y. Motion control in an electric vehicle with four independently driven in-wheel motors. *IEEE/ASME Trans. Mechatron.* **1999**, *4*, 9–16.
4. Hori, Y. Future vehicle driven by electricity and control-research on four-wheel-motored “UOT electric march II”. *IEEE Trans. Ind. Electron.* **2004**, *51*, 954–962.
5. Dejun, Y.; Oh, S.; Hori, Y. A novel traction control for EV based on maximum transmissible torque estimation. *IEEE Trans. Ind. Electron.* **2009**, *56*, 2086–2094.
6. Deur, J.; Pavkovic, D.; Burgio, G.; Hrovat, D. A model-based traction control strategy non-reliant on wheel slip information. *Veh. Syst. Dyn.* **2011**, *49*, 1245–1265.
7. Magallan, G.A.; de Angelo, C.H.; Garcia, G.O. Maximization of the traction forces in a 2WD electric vehicle. *IEEE Trans. Veh. Technol.* **2011**, *60*, 369–380.
8. Yan, C.; Wang, J. Adaptive energy-efficient control allocation for planar motion control of over-actuated electric ground vehicles. *IEEE Trans. Control Syst. Technol.* **2014**, *22*, 1362–1373.
9. Yin, G.; Wang, R.; Wang, J. Robust control for four wheel independently-actuated electric ground vehicles by external yaw-moment generation. *Int. J. Automot. Technol.* **2015**, *16*, 839–847.
10. Subudhi, B.; Ge, S.S. Sliding-mode-observer-based adaptive slip ratio control for electric and hybrid vehicles. *IEEE Trans. Intell. Transp. Syst.* **2012**, *13*, 1617–1626.
11. Mirzaeinejad, H.; Mirzaei, M. A novel method for non-linear control of wheel slip in anti-lock braking systems. *Control Eng. Pract.* **2010**, *18*, 918–926.
12. Amodeo, M.; Ferrara, A.; Terzaghi, R.; Vecchio, C. Wheel slip control via second-order sliding-mode generation. *IEEE Trans. Intell. Transp. Syst.* **2010**, *11*, 122–131.

13. Fazeli, A.; Zeinali, M.; Khajepour, A. Application of adaptive sliding mode control for regenerative braking torque control. *IEEE/ASME Trans. Mechatron.* **2012**, *17*, 745–755.
14. Castro, R.; Araujo, R.E.; Freitas, D. Wheel slip control of EVs based on sliding mode technique with conditional integrators. *IEEE Trans. Ind. Electron.* **2013**, *60*, 3256–3271.
15. He, H.; Peng, J.; Xiong, R.; Fan, H. An Acceleration slip regulation strategy for four-wheel drive electric vehicles based on sliding mode control. *Energies* **2014**, *7*, 3748–3763.
16. Johansen, T.A.; Petersen, I.; Kalkkuhl, J.; Ludemann, J. Gain-scheduled wheel slip control in automotive brake systems. *IEEE Trans. Control Syst. Technol.* **2003**, *11*, 799–811.
17. Savaresi, S.M.; Tanelli, M.; Cantoni, C. Mixed slip-deceleration control in automotive braking systems. *J. Dyn. Syst. Meas. Control* **2007**, *129*, 20–31.
18. Choi, S.B. Antilock brake system with a continuous wheel slip control to maximize the braking performance and the ride quality. *IEEE Trans. Control Syst. Technol.* **2008**, *16*, 996–1003.
19. Pasillas-Lepine, W.; Loria, A.; Gerard, M. Design and experimental validation of a nonlinear wheel slip control algorithm. *Automatica* **2012**, *48*, 1852–1859.
20. Mirzaei, M.; Mirzaeinejad, H. Optimal design of a non-linear controller for anti-lock braking system. *Transp. Res. Part C Emerg. Technol.* **2012**, *24*, 19–35.
21. Unsal, C.; Kachroo, P. Sliding mode measurement feedback control for antilock braking systems. *IEEE Trans. Control Syst. Technol.* **1999**, *7*, 271–281.
22. Goggia, T.; Sorniotti, A.; De Novellis, L.; Ferrara, A.; Gruber, P.; Theunissen, J.; Steenbeke, D.; Knauder, B.; Zehetner, J. Integral sliding mode for the torque-vectoring control of fully electric vehicles: Theoretical design and experimental assessment. *IEEE Trans. Veh. Technol.* **2015**, *64*, 1701–1715.
23. Gerard, M.; Pasillas-Lépine, W.; De Vries, E.; Verhaegen, M. Improvements to a five-phase ABS algorithm for experimental validation. *Veh. Syst. Dyn.* **2012**, *50*, 1585–1611.
24. Savaresi, S.M.; Tanelli, M. *Active Braking Control Systems Design for Vehicles*; Springer-Verlag: New York, NY, USA, 2010.
25. Rajamani, R. *Vehicle Dynamics and Control*; Springer-Verlag: New York, NY, USA, 2005.
26. Slotine, J.J.E.; Li, W. *Applied Nonlinear Control*; Prentice-Hall: Englewood Cliffs, NJ, USA, 1991.
27. Nam, K.; Fujimoto, H.; Hori, Y. Design of an adaptive sliding mode controller for robust yaw stabilisation of in-wheel-motor-driven electric vehicles. *Int. J. Veh. Des.* **2015**, *67*, 98–113.
28. Nam, K.; Fujimoto, H.; Hori, Y. Lateral stability control of in-wheel-motor-driven electric vehicles based on sideslip angle estimation using lateral tire force sensors. *IEEE Trans. Veh. Technol.* **2012**, *61*, 1972–1985.
29. Kobayashi, K.; Cheok, K.C.; Watanabe, K. Estimation of absolute vehicle speed using fuzzy logic rule-based Kalman filter. In Proceedings of the American Control Conference, Seattle, WA, USA, 21–23 June 1995; pp. 3086–3090.
30. Daiss, A.; Kiencke, U. Estimation of vehicle speed fuzzy-estimation in comparison with Kalman-filtering. In Proceedings of the 4th IEEE Conference on Control Applications, New York, NY, USA, 28–29 September 1995.

31. Jiang, F.; Gao, Z. An adaptive nonlinear filter approach to the vehicle velocity estimation for ABS. In Proceedings of the 2000 IEEE International Conference on Control Applications, Anchorage, AK, USA, 25–27 September 2000; pp. 490–495.
32. Lars, I.; Tor, A.J.; Thor, I.F.; Håvard, F.G.; Jens, C.K.; Avshalom, S. Vehicle velocity estimation using nonlinear observers. *Automatica* **2006**, *42*, 2091–2103.
33. Ljung, L. *System Identification: Theory for the User*; Prentice-Hall: Englewood Cliffs, NJ, USA, 1987.

© 2015 by the authors; licensee MDPI, Basel, Switzerland. This article is an open access article distributed under the terms and conditions of the Creative Commons Attribution license (<http://creativecommons.org/licenses/by/4.0/>).